Arabian Journal of Chemistry (2023) **16**, 104481

King Saud University

**Arabian Journal of Chemistry**

www.ksu.edu.sa
www.sciencedirect.com

ORIGINAL ARTICLE

# Synthesis of nickel cobalt-codoped tin oxide nanoparticles from *Psidium guajava* with anticancer properties

**Abozer Y. Elderdery [a,b,*], Badr Alzahrani [a], Abdulrahim A. Alabdulsalam [c], Fehaid Alanazi [d], Siddiqa M A Hamza [e], Ahmed M E Elkhalifa [f,g], Abdulaziz H. Alhamidi [h], A. Mohamedain [c,i], Suresh Kumar Subbiah [j], Pooi Ling Mok [k]**

[a] *Department of Clinical Laboratory Sciences, College of Applied Medical Sciences, Jouf University, Sakaka, Saudi Arabia*
[b] *Health Sciences Research Unit, Jouf University, Sakaka, Saudi Arabia*
[c] *Department of Biomedical Sciences, College of Medicine, King Faisal University, Alhofuf, Saudi Arabia*
[d] *Department of Clinical Laboratory Sciences, College of Applied Medical Sciences-AlQurayyat, Jouf University, Saudi Arabia*
[e] *Faculty of Medicine, Department of Pathology, Umm Alqura University, Algunfuda, Saudi Arabia*
[f] *Department of Public Health, College of Health Sciences, Saudi Electronic University, Riyadh, Saudi Arabia*
[g] *Department of Haematology, Faculty of Medical Laboratory Sciences, University of El Imam El Mahdi, Kosti, Sudan*
[h] *Clinical Laboratory Sciences Department, College of Applied Medical Science, King Saud University, Riyadh, Saudi Arabia*
[i] *Department of Biochemistry, Faculty of Medicine, Khartoum University, Sudan*
[j] *Centre for Materials Engineering and Regenerative Medicine, Bharath Institute of Higher Education and Research, Chennai, India*
[k] *Department of Biomedical Sciences, Faculty of Medicine & Health Sciences, Universiti Putra Malaysia, 43400 UPM Serdang, Selangor, Malaysia*

Received 25 June 2022; accepted 28 November 2022
Available online 5 December 2022

**KEYWORDS**

Acute lymphoblastic leukemia (ALL);
Antibacterial;
Anticancer;

**Abstract** Metal oxide nanoparticles have been found to selectively target the tumor cells while non-toxic to the normal cells. Leukemia is one of the widespread and deadly cancers in adults, as well as the most common cancer in children. Recently, the nanoparticles have evolved as a simple, economic, effective, and ecologically sound strategy among the known nanoparticle synthesis techniques. In the present study, the structural, optical, and antibacterial effects of nickel cobalt-

* Corresponding author at: Jouf University, Saudi Arabia.
E-mail address: ayelderdery@ju.edu.sa (A.Y. Elderdery).
Peer review under responsibility of King Saud University.

Production and hosting by Elsevier

https://doi.org/10.1016/j.arabjc.2022.104481
1878-5352 © 2022 The Authors. Published by Elsevier B.V. on behalf of King Saud University.
This is an open access article under the CC BY-NC-ND license (http://creativecommons.org/licenses/by-nc-nd/4.0/).

Green Synthesis;
*Psidium guajava*;
SnNiCoO2 NPs

codoped Tin oxide nanoparticles (SnNiCoO2 NPs) formulated by the green process and the anti-cancer potential of SnNiCoO2 NPs in Molt-4 cells have been studied. The cytotoxic potential of the NPs against Molt-4 cells was estimated by MTT assay. The ROS and MMP levels were measured using fluorescent dyes and the changes in morphology and nuclei were noted using AO/EB staining. CAT, SOD, MDA, and GSH), and Proinflammatory Cytokines (TNF-α and IL1β) were also studied. The activity of caspase-3, −9, and −8 levels was examined to analyze the apoptotic mechanism. The XRD patterns of SnNiCoO2 NPs revealed a tetragonal structure. The SnNiCoO2 NPs was revealed a diameter of 126 nm by the DLS study. The morphology and elemental composition were studied using FESEM and EDAX spectra. In the FT-IR study, the O-sn-O stretching band was found to be 615 and 542 cm-1. The antimicrobial potential of the SnNiCoO2 NPs was examined against S. aureus, E. coli, and C. Albicans strains. A tremendous reduction in the viability of MOLT-4 cells at concentration-dependent mode witnessed the cytotoxic potential of the formulated NPs. The augmented ROS accumulation, depletion of MMP status, depleted antioxidants, and increased proinflammatory cytokines (TNF-α and IL1β) were noted on the NPs exposed cells. Furthermore, the increased expressions of caspase-3, −9, and −8 was also noted in the NPs treated MOLT-4 cells. Hence, the outcomes suggest that the formulated SnNiCoO2 NPs had remarkably potent antimicrobial and anticancer properties and could potentially prove beneficial in cancer treatment. Induces mitochondrial oxidative stress with nickel–cobalt-codoped tin oxide nanoparticles from *Psidium guajava*, which is a potential drug candidate for the antibiotic, antifungal, and anticancer activities of plant-based nanoparticles.

© 2022 The Authors. Published by Elsevier B.V. on behalf of King Saud University. This is an open access article under the CC BY-NC-ND license (http://creativecommons.org/licenses/by-nc-nd/4.0/).

## 1. Introduction

Acute lymphoblastic leukemia (ALL) is a blood tumor characterized by lymphatic tissue propagation and aberrant differentiation in the peripheral blood, bone marrow, and several other tissues (Iyappan et al., 2021). It impacts both children and adults, with a peak incidence between the ages of 2 and 5 (Nikbakht et al., 2017). Despite significant advancements in treatment for ALL patients, recurrence continues to be a major concern for these individuals (Bahmani et al., 2018). The currently available therapeutic medications used to treat ALL have a variety of side effects, including peripheral neuropathy, drug resistance, and immune system suppression (Chao et al., 2015). As a result, searching for alternative anti-cancer medicines that are both safe and effective is a critical importance.

Nanotechnology has evolved into a influential and innovative area of study over the last few decades, focusing on the application of nanomaterials in areas such as health care, biomedicine, and drug delivery (Ahmed et al., 2017). The development of semiconducting metal oxide nanoparticles is potentially essential because of their peculiar physical–chemical features and applicability in areas such as nanoelectronics, catalysis, optoelectronics, photonic devices, storage devices, and biomedical technology (Chavali et al., 2019; Pal et al., 2021; Khan et al., 2021). In addition to having a wide *n*-type bandgap, $SnO_2$ nanoparticles exhibit high clarity, high carrier density, chemical stability, and thermal stability at 300 K, making them a key *n*-type semiconductor (Srinivas et al., 2009; Agrahari et al., 2015; Pascariu et al., 2016).

The ability to synthesize nanostructured materials with small dimensions and precise structures is potentially critical for biomedical applications. Recent decades have witnessed extensive research on the medical characteristics of SnO2 NPs semiconductors. The optical characteristics of the material change as the size of the material reduces and the bandgap widens, allowing it to be utilized in novel biomedical applications. The changes in the optical properties of the metal oxide semiconductor, employed by impurity atoms, or doping is a extensively established technique (Bhuvana et al., 2017; Mostafa et al., 2020). Divya et al. (2020) highlighted that Cu and Ni-doped SnO2 NPs were improved by magnetic and electrical conductivity (Divya et al., 2020). The anti-bacterial property of Ni, Fe, and Ni–Fe co-doped SnO2 NPs was enhanced as compared with the SnO2 NPs, which can be ascribed to ROS generation and the nanoscale dimension of the particles (Amutha et al., 2019). Though, in best of our understanding, optical and antibacterial effects have not been found for SnNiCoO2 NPs.

Recently, nanoparticles (NPs) have received great interests owing to their potential applications in cancer treatment (Prashanth et al., 2018). Among all the available methods of nanoparticle synthesis, the biological approach is highly favored over other approaches as it is a simple, environmentally friendly, sustainable, and reproducible procedure that often leads to a stable nanoparticle formation (Chakravarty et al., 2016; Mittal et al., 2014). A significant amount of research into employing various portions of plants for NPs synthesis has increased, as plants are readily accessible, provide a greater yield, and encompass a range of phytochemicals that can reduce a range of metal oxides and lead to NP formation in a brief period (Abdelghany et al., 2018; Khan et al., 2021; Ghramh et al., 2019). Moreover, various reports have linked the role of secondary metabolites like phenols, carbohydrates, saponins, tannins, flavonoids, and terpenoids as both reducing and stabilizing agents in the formation of metallic NPs (Basnet et al., 2018).

*Psidium guajava* L. (*P. guajava*) is a popular herbal plant spread throughout Asia and belongs to the Myrtaceae family (Wang et al., 2018). The plant leaves possess several pharmacologically active substances such as gallic acid, catechin, and kaempferol (Suwan et al., 2019). Moreover, they exhibit numerous significant biological effects including anti-inflammatory activity, hepatoprotective effect, antimicrobial and antioxidant activity, anti-hyperglycemic, and anti-hyperlipidemic effects (Barbalho et al., 2012; Nguyen et al., 2020).

The purpose of this investigation is to assess the structural, optical, and antibacterial effects of nickel–cobalt-codoped Tin oxide nanoparticles produced via a green approach and to examine the anti-cancer potential of SnNiCoO2 NPs in human leukemic cells. The cytotoxic potential of the NPs against Molt-4 cells was estimated by MTT assay. The MMP and ROS levels were detected using fluorescent dyes. The alterations in nuclei and morphology was observed using AO/EB staining. The activity of caspase-3, −9, and −8 levels was examined to analyze the apoptotic mechanism.

## 2. Materials and methods

### 2.1. Experimental methods

#### 2.1.1. Green synthesis of $SnNiCoO_2$ NPs

The $SnNiCoO_2$ NPs were fabricated by the green route approach. First, the 0.002 M of nickel nitrate solution and Cobalt nitrate solution of 0.002 M was added into an aqueous tin chloride solution of 0.094 M. Then, 100 mL of Psidium guajava leaf extract was mixed to the solution, and magnetically agitated for 20 min to produce a homogenous green solution. The resulting solution was then microwaved at 800 W for 10 min in autoclave bottles with polypropylene caps and then cooled to 37 °C and cleansed many times using deionized water and ethanol. The obtained residue was dehydrated at 120 °C, and a light white powder was obtained. Finally, $SnNiCoO_2$ NPs were calcinated at 800 °C for 5 h and then used for further analysis.

#### 2.1.2. Characterization techniques

A model X'PERT PRO PANalytical X-ray diffractometer was used to characterize the SnNiCoO2 NPs. Using a monochromatic wavelength of 1.54 Å, the diffraction patterns of SnNiCoO2 NPs were recorded over the range of 25°-80°. FE-SEM (Carl Zeiss Ultra 55 FESEM) with EDTA (model: Inca) was utilized to examine the morphology of the samples. Perkin-Elmer spectrometers were utilized to determine FT-IR spectrum at 400–4000 cm-1 ranges. JASCO spectrofluorometer FP-8200 was utilized to investigate the photoluminescence emission spectrum.

#### 2.1.3. Antibacterial assays

In the diffusion method, the antibacterial property of the SnNiCoO2 NPs was investigated against bacterial species i.e., *E. coli* and *S. aureus* in agar plates. By spreading 100 mL of a freshly cultured bacterium that contained $1 \times 10^8$ CFU/mL onto agar plates, the bacteria were characterized. SnNiCoO2 nanoparticles dispersed in dimethyl sulphoxide (DMSO) were examined at 1, 1.5, and 2 mg/ml dosages on the perti plate. We determined the zone of inhibition levels (mm) for 24 h at 37 °C. Amoxicillin (10 µg disc) was utilized as standard.

#### 2.1.4. Antifungal assays

*C. Albicans* was tested using potato dextrose agar with a good diffusion method to determine antifungal activity. After the strains were spread over PDA plates, it was incubated at 30 °C for 30 min. After that, the test samples (SnNiCoO2 NPs) were loaded into sterile forceps and subsequently incubated under visible light at 30 °C for 24 h. 24 h was measured at 37 °C for the zone of inhibition (mm). For the positive control, amphotericin B was used.

### 2.2. Chemicals

Trypsin-EDTA, Streptomycin, Penicillin, FBS, buffered saline, 2′-7′dichlorofluorescin diacetate (DCFH-DA), Rhodamine-123 (Rh-123) dye, and 3-(4,5-Dimethylthiazol-2-yl)-2,5-diphe nyltetrazolium bromide (MTT) was acquired from Sigma-Aldrich (USA).

### 2.3. Cell culture

Human ALL (Molt-4) cells were obtained from American Type Culture Collection, USA and grown on a DMEM media enriched with 10 % FBS and sustained at 37 °C with 98 % humidity in $CO_2$ incubators.

### 2.4. MTT cytotoxicity assay

An approach developed by Mosmann, (1983) was used to assess the cytotoxicity of the NPs on Molt-4 cells. The cells were loaded onto the 96-well plates and exposed for 24 h with $SnNiCoO_2$ NPs (10–60 µg/ml). Then, 20 mL MTT dye (2.5 mg/ml) was added and left for 4 h. DMSO (150 µl) was then mixed to the solution and the crystals were suspended in it and then the absorbance was tested at 570 nm. It was determined that viability was 50 % at an inhibitory concentration (IC50).

### 2.5. H2DCF-DA ROS detection assay

The Molt-4 cells were used to measure ROS, and the method used was Chen et al. (2013) with minimal changes. In a 96 well plate, cells were grown at $6X10^4$ cells per well and sustained for 24 h. Later, cells were administered with 40 and 50 g/ml concentrations of green Nickel cobalt-*co*-doped Tin oxide nanoparticles (SnNiCoO2 NPs). Following a 24-hour incubation period, 10 µM H2DCF-DA was mixed for 30 min in the dark. The fluorescence at 485 and 535 nm for excitation and emission, respectively was measured and fluorescent images were taken using a fluorescent microscope.

### 2.6. Measurement of MMP

In a 6-well plate, the cells were left for incubation for 24 h with $SnNiCoO_2$ NPs (40 and 50 µg/ml). Rh-123 is a fluorescent dye that is employed to assess MMP depolarization. The dye was added to the wells at 37 °C for 30 min then cleansed with PBS and viewed under a fluorescent microscope. Image J software was employed to investigate the fluorescence strength of the recorded images and a blue filter (450–490 nm) was utilized to capture the intensity.

### 2.7. Determination of caspases −8, −9, and −3 activities

The treatment of $SnNiCoO_2$ NPs with Molt-4 cells was carried out and incubated for 24 h. The caspase activities were detected using a assay kits as per the manufacturer's guidelines (Invitrogen, USA). Each kit provides a particular substrate for caspases −3, −8, and −9: Ac-DEVD (acetyl-AspGlu-Val-Asp), IETD (Ile-GluThr-Asp), and LEHD (Leu-Glu-His-Asp), which was tagged with the chromophore p-nitroanilide (pNA), which gets liberated when active caspases cleave them and further quantified in a spectrophotometer at 405 nm (Biotek Instruments EL800, USA).

### 2.8. Statistical analysis

The data are revealed as a mean ± SD of triplicates. The SPSS V 17 software was utilized to determine the statistical tests

(SPSS Inc, 2008). The significance was determined using one-way ANOVA and the DMRT test. If $p < 0.05$, the results are deemed statistically significant.

## 3. Results

### 3.1. Characterization of green $SnNiCoO_2$ NPs

The XRD pattern of green $SnNiCoO_2$ NPs is depicted in Fig. 1a. The $SnNiCoO_2$ NPs diffraction peaks at 2θ = 26.05, 33.31, 37.42, 38.39, 51.21, 54.21, 57.34, 61.36, 64.27, 65.37, 70.71 and 78.20 respectively. Which corresponding hkl planes are (110), (101), (200), (111), (211), (220), (002), (310), (112), (301), (202), and (321) for $SnNiCoO_2$ NPs. The prepared $SnNiCoO_2$ NPs exhibit a rutile structure. It is perfectly matched with standard diffraction peaks of $SnO_2$ NPs (JCPDS 77–0450). The Scherrer equation ($D = K\lambda/(\beta\cos\theta)$) was used to compute the average size, where λ-is the X-ray wavelength, D is the grain size, K is the constant 0.89, β-is the full-wave half-maximum width of the diffraction peak and θ is the diffraction angle (Naje et al., 2013). $SnNiCoO_2$ NPs exhibited an average crystalline size of 65 nm.

Fig. 1b illustrates the particle size distribution of the $SnNiCoO_2$ NPs, which is investigated by DLS study. The $SnNiCoO_2$ NPs revealed average size of 126 nm. However, DLS particle size was increased than the XRD results owing to the reason that $SnNiCoO_2$ NPs were enclosed by an aqueous medium.

#### 3.1.1. The morphology and elemental mapping of $SnNiCoO_2$ NPs:

The surface morphology and elemental mapping were investigated by EDAX spectrum, and FESEM are revealed in (Fig. 2a, 2b, and 3). The FE-SEM images of $SnNiCoO_2$ NPs were found to be spherical with uniformly sized particles and an average size of 65 nm. From the EDAX spectra, the atomic percentage of Sn, Ni, Co, and O were observed at 19.53 %, 0.60 %, 0.55 %, and 79.32 %, respectively. The element mapping observed for $SnNiCoO_2$ NPs and uniform distribution of elements was (Sn, Ni, Co, and O) throughout the material.(See Fig. 3).

#### 3.1.2. Spectral analysis of $SnNiCoO_2$ NPs

FTIR spectra of the $SnNiCoO_2$ NPs are revealed in Fig. 4a. The functional groups of the biomolecules are important for reducing $SnNiCoO_2$ NPs. The broad O—H stretching bands were noted at 3423 $cm^{-1}$, corresponding to the re-adsorption of water from the ambient atmosphere (Khojasteh et al., 2022). The symmetric and asymmetric peak was observed for C—H at 2920 cm-1 and a small peak for sn-OH at 1092 cm-1. It was found that the broad metal oxide (M−O−M) stretching bands were 615 and 542 cm-1 that is due to the sn-O-Sn stretching mode of the surface-bridging oxide generated upon compression of neighboring hydroxyl groups present on the surface (Rani et al., 2021).

Fig. 4b demonstrates the photoluminescence spectra of $SnNiCoO_2$ NPs. Excitation peaks were noted at 325 nm,

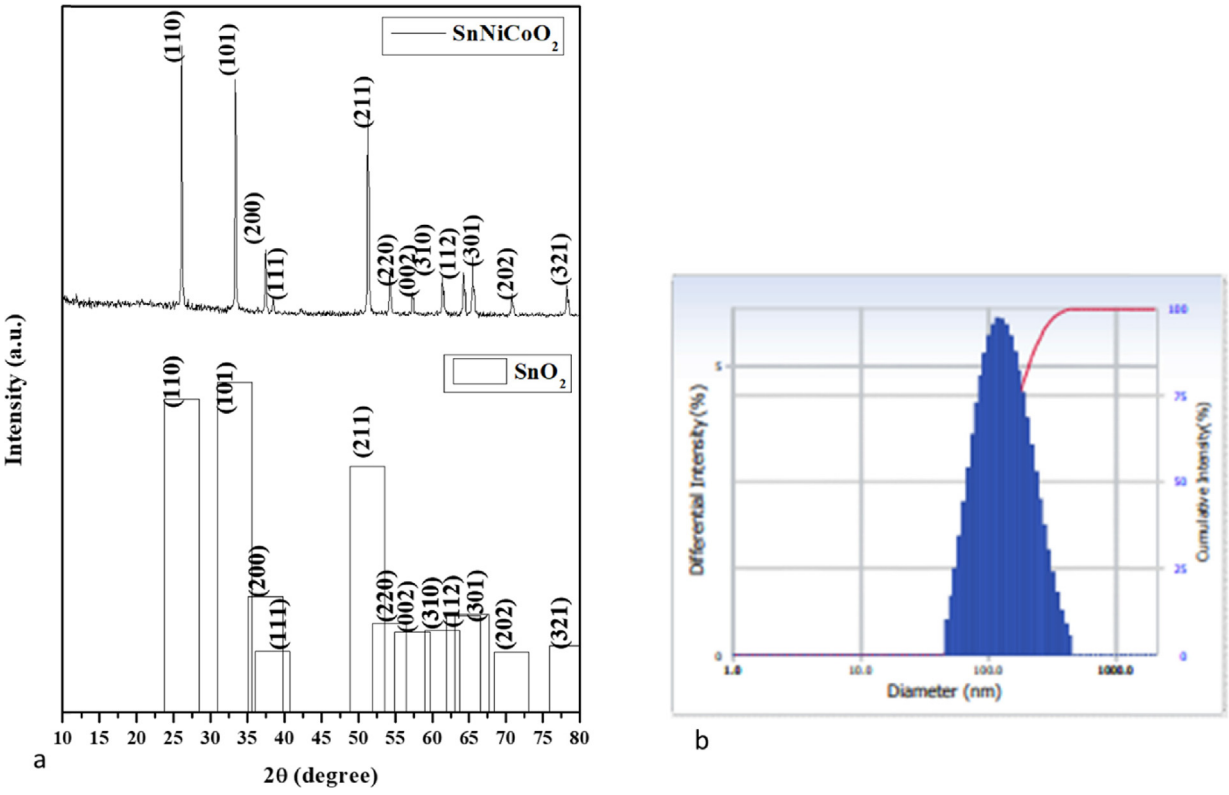


**Fig. 1** XRD Pattern of SnNiCoO2 NPs (a). Number-weighted particle size distribution, obtained by DLS (b).

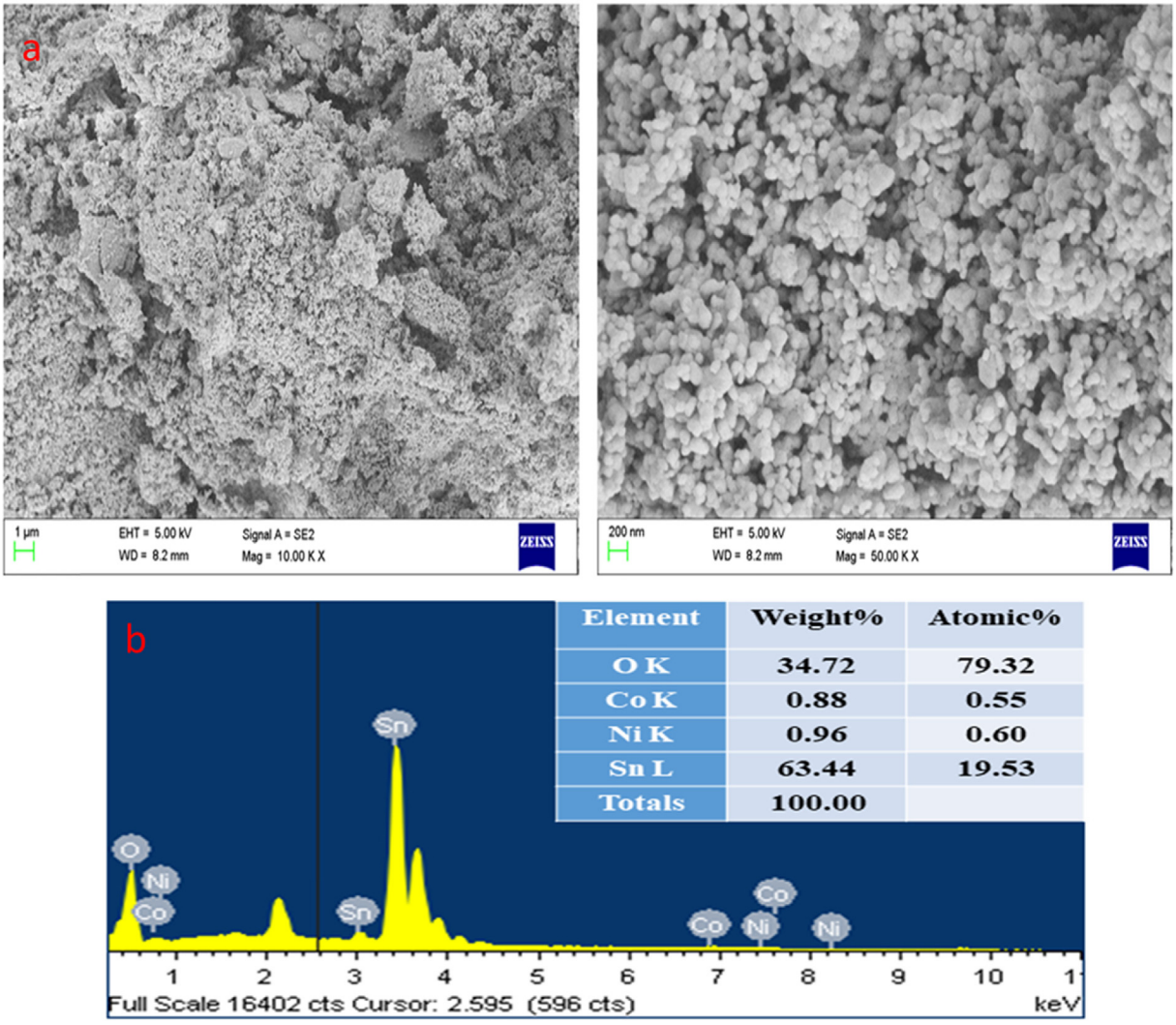


**Fig. 2** FESEM micrographics of the SnNiCoO2 NPs: Lower and Higher magnification FESEM image (a). Elements, weight %, and atomic % of the composition were obtained by EDX (b).

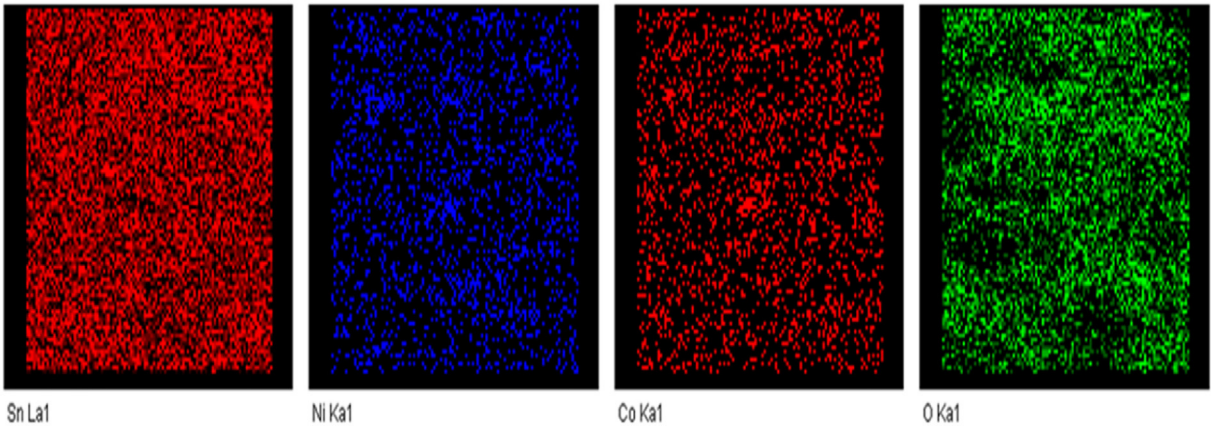


**Fig. 3** Elemental mapping spectrum of $SnNiCoO_2$ NPs.

399 nm, 421 nm, 436 nm, 454 nm, 479 nm, 489 nm, 522 nm, and 527 nm, and emission peaks were noted at 367 nm, 399 nm, 421 nm, 436 nm, 454 nm, 479 nm, 489 nm, 522 The recombination of the electron from the Sn 4p conduction band to the hole in the O 2p valance band is responsible for the two UV emission peaks at 367 nm and 399 nm (Sephra et al., 2016). The intrinsic states localized on the $SnO_6$ octahedral are responsible for the violet emission peak at 421 nm (Toloman

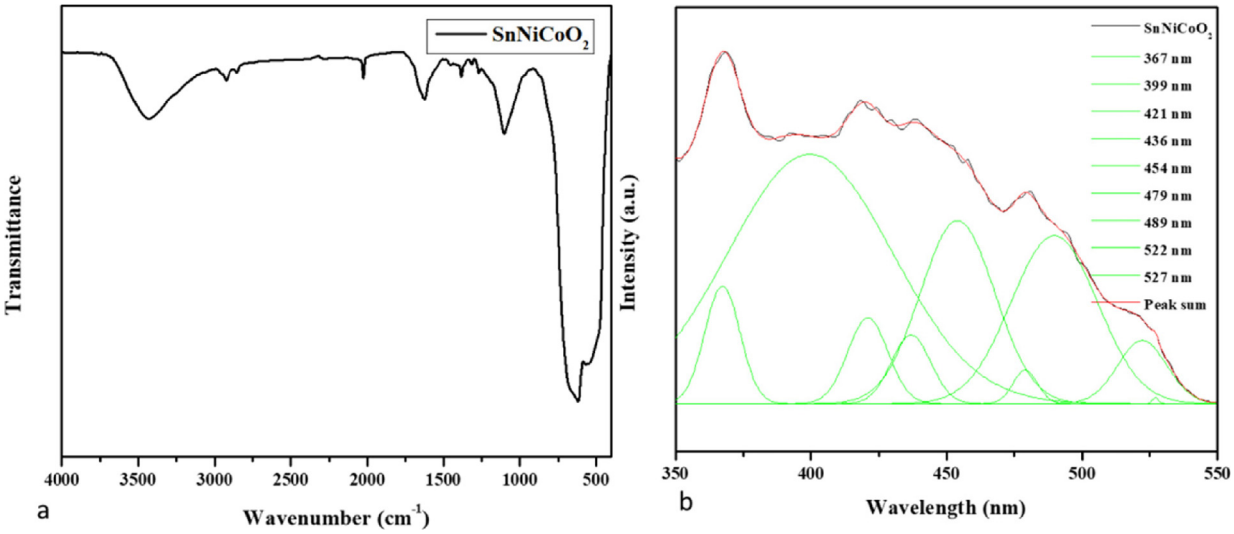


**Fig. 4** Spectral analysis of SnNiCoO2 NPs. FTIR Transmittance vs wavenumber chart of SnNiCoO2 NPs derived from infrared analysis (a). Photoluminescence spectra for SnNiCoO2 NPs at room temperature (b).

et al., 2020). The tin interstitials or dangling $SnO_2$ nanoparticles are responsible for the violet-blue emission peaks at 436 nm. At 454 nm, 479 nm, and 489 nm, the blue emission peaks correspond to an oxygen vacancy. Green emission peaks at 522 and 527 nm have been attributed to oxygen vacancy with trapped electrons (Sephra et al., 2016; Toloman et al., 2020).

### 3.2. Antimicrobial activity of the $SnNiCoO_2$ NPs

The antibacterial property of $SnNiCoO_2$ NPs was confirmed against *S. aureus* and *E. coli* bacteria, as well as *C. Albicans* fungi (Fig. 5). In comparison to conventional antibiotics, $SnNiCoO_2$ NPs have the highest antibacterial activity. Amoxicillin has a lot of antibacterial power. As the concentration of SnNiCoO2 NPs increased, so did the zone of inhibition.

### 3.3. Impact of $SnNiCoO_2$ NPs on the cell viability

The cytotoxicity of $SnNiCoO_2$ NPs on Molt-4 cells are revealed in Fig. 6. The cells treated with $SnNiCoO_2$ NPs exhibited considerable reduction in the viability at dose-dependent manner. A bright-field phase-contrast microscope was employed to determine the morphological changes in

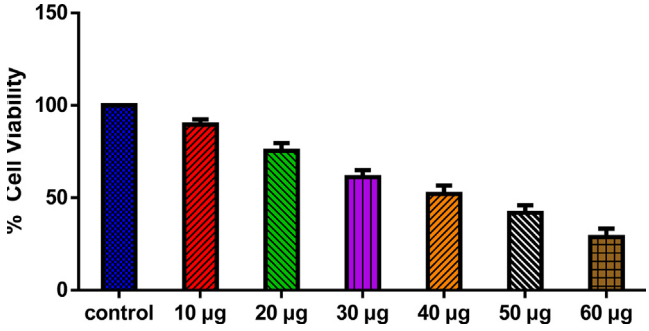


**Fig. 6** SnNiCoO2 NPs cause cytotoxicity in MOLT-4 cells. MOLT-4 cell lines were treated with different concentrations (10 – 60 µg/ml) of SnNiCoO2 NPs for 24 h. The cells were subjected to an MTT assay and the values were depicted as ± SD of three individual experiments.

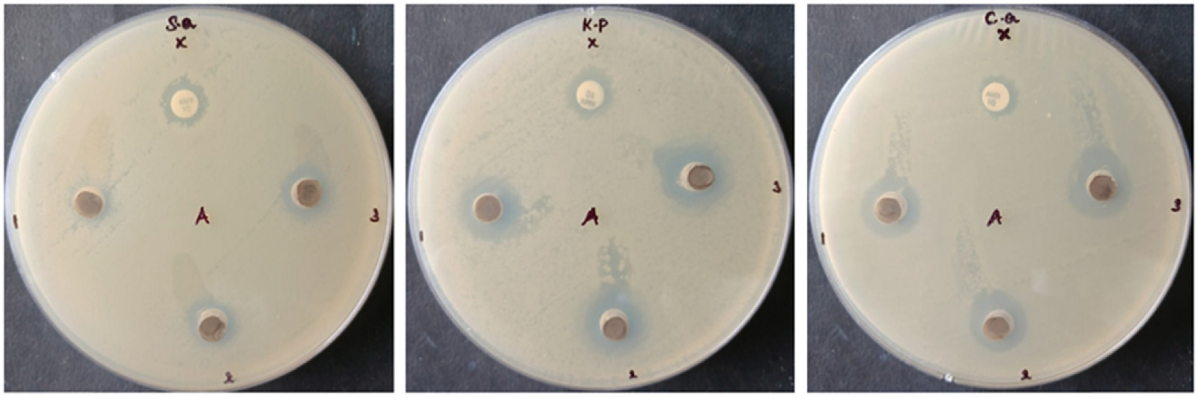


**Fig. 5** Antimicrobial activity of SnNiCoO2 NPs. NMs of CeO2 inhibit the growth of *S. aureus, K. Pneumonia,* and *C. albicans.*

Molt-4 cells. At the 40 µg/ml dose, $SnNiCoO_2$ NPs exposure led to a considerable depletion of cell viability and distracted morphology, and with higher dosages, increased alterations in the morphology was noted. With the 50 µg/ml of $SnNiCoO_2$ NPs (IC50) substantially reduced the viability after 24 h. As a result, 40 and 50 µg/ml of $SnNiCoO_2$ NPs were selected for additional studies.

### *3.4. Impact of $SnNiCoO_2$ NPs induced apoptosis*

The dual (AO/EtBr) staining approach was performed to study the apoptosis in the $SnNiCoO_2$ NPs administered MOLT-4 cells. The control cells showed higher green fluorescence; however, the $SnNiCoO_2$ NPs treated cells showed a strong orange fluorescence stained by EtBr, indicating that they were apoptotic (Fig. 7). As a result, it became obvious that $SnNiCoO_2$ NPs could induce apoptosis in blood cancer cells.

### *3.5. Detection of intracellular ROS accumulation in treated cells*

DCFH-DA staining was performed to examine ROS accumulation in Molt-4 cells exposed to $SnNiCoO_2$ NPs (40 and 50 µg/ml). We measured ROS production in H2-DCFDA-loaded cells using a fluorescent microscope after exposing $SnNiCoO_2$ NPs (40, 50 µg/mL) for 24 h. The outcomes revealed that cells exposed to $SnNiCoO_2$ NPs (40, 50 µg/mL) for 24 h produced significantly more ROS when compared with untreated cells. The bright green fluorescence revealed the presence of ROS (Fig. 8). Molt-4 cells administered with $SnNiCoO_2$ NPs (40 µg/ml) demonstrated high fluorescence, but those exposed with greater dose of $SnNiCoO_2$ NPs (50 µg/ml) revealed higher green fluorescence, signifying an augmented ROS accumulation.

### *3.6. Determination of MMP level in the treated cells*

Rh-123 staining was performed to monitor the MMP status in the $SnNiCoO_2$ NPs (40 and 50 µg/ml) exposed Molt-4 cells, and the results are depicted in Fig. 9. It was discovered that control cells exhibited a bright green fluorescence, but Molt-4 cells exposed with $SnNiCoO_2$ NPs exhibited the depleted green fluorescence, which signifying the decrease in MMP. This outcome exhibited that $SnNiCoO_2$ NPs can deplete MMP status in Molt-4 cells (Fig. 9).

### *3.7. Detection of caspase −3, −9, and −8 activities*

The expression of pro-apoptotic proteins in untreated and $SnNiCoO_2$ NPs treated cancer cells is shown in Fig. 10. Caspases-3, −8, and −9 expressions were all downregulated in control cells. The $SnNiCoO_2$ NPs exposed Molt-4 cells exhibited higher expressions of caspase-3, −9, and −8 as than untreated cells. $SnNiCoO_2$ NPs considerably augmented the expression of pro-apoptotic biomarkers.

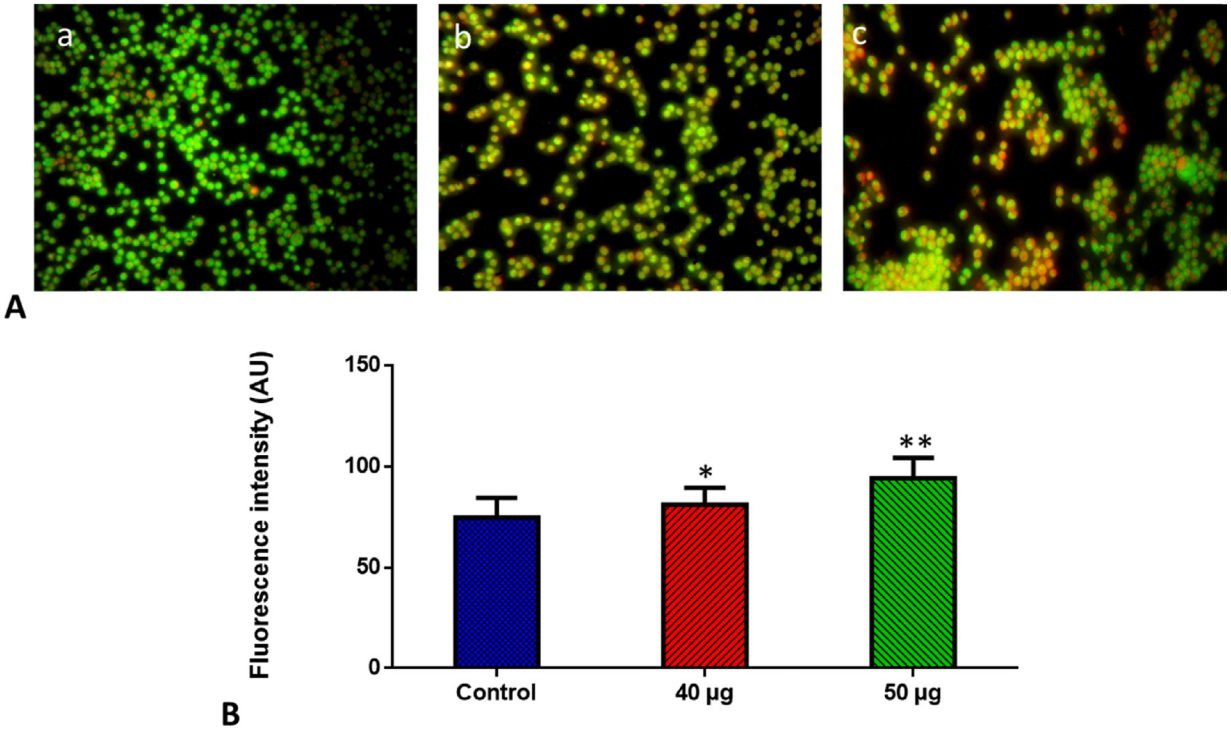


**Fig. 7** Effect of SnNiCoO2 NPs on the apoptotic cell death in the blood cancer MOLT-4 cells for 24 h. Acridine orange and ethidium bromide (1:1), was used to stain the cells, then analyzed by fluorescence microscopy (Labomed, USA). The control cells showed green fluorescence that indicates living cells without apoptosis. The SnNiCoO2 NPs tested cells showed yellow and orange fluorescence, which indicates early and late apoptotic cell death, respectively with condensed or fragmented nuclei and necrotic cells. Panel A; Control (a) (untreated cells), SnNiCoO2 NPs-treated cells; 40 µg/ml concentration (b) and 50 µg/ml concentration (c). Panel B; Arbitrary Units (a.u.) of fluorescent Intensity from the control and treated cells incubated at 37 °C were measured by a fluorescence microplate reader. *$p < 0.05$ compared to the "Control" group and **$p < 0.005$ compared to the "Control" group.

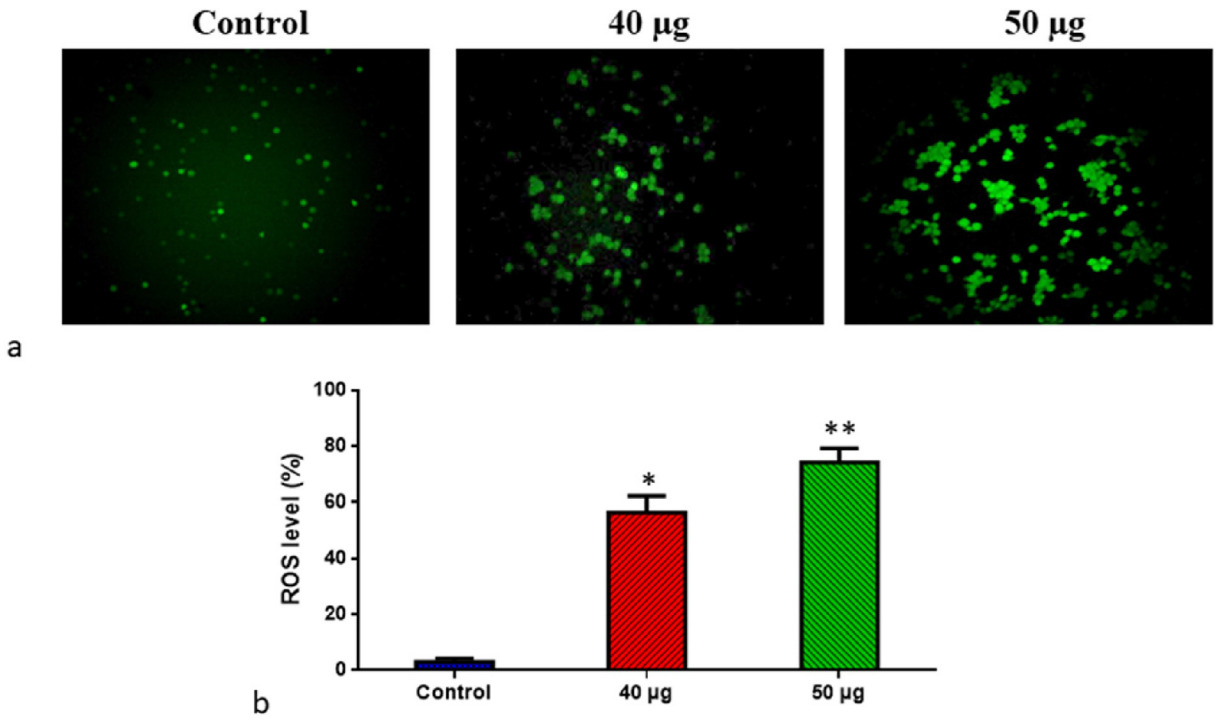


**Fig. 8** Effect of SnNiCoO2 NPs on the intracellular ROS generation in the blood cancer MOLT-4 cells. The MOLT-4 cell line is subjected to oxidative stress induced by SnNiCoO2 NPs staining with DCFH-DA. Then the digital images were captured by a Fluorescence microscope (Labomed, USA). Control cells showed a dull green fluorescence that indicates poor ROS generation. The SnNiCoO2 NPs (40 and 50 µg/ml) treated cells showed a bright green fluorescence, which confirms the increased ROS production in MOLT-4 cells. (a); Control (untreated cells), SnNiCoO2 NPs-treated cells; 40 µg/ml concentration and 50 µg/ml concentration. (b); ROS levels in percentage from the control and treated cells incubated at 37 °C were measured by a fluorescence microplate reader using the H2DCFDA dye. *$p < 0.05$ compared to the "Control" group and **$p < 0.005$ compared to the "Control" group.

## 4. Discussion

Plant products have been popularly employed in nanobiotechnology in the past few years. A high number of phytochemicals present in *P. guajava* extract has been reported to possess excellent reducing power (Suwan et al., 2019; Antony et al., 2013). Transition metal NPs are receiving immense popularity owing to their excellent characteristics such as biocompatibility, minimal toxicity, and low ecological impact (Elango et al., 2015; Alserihi et al., 2022; Tabrez et al., 2022(a)). Moreover, a few metal oxide NPs can specifically target tumor cells with lesser toxicity than normal cells (Ahamed et al., 2018; Ullah et al., 2022; Gowd et al., 2022). Consequently, the purpose of this exploration was to assess the structural, optical, and antibacterial activities of nickel–cobalt-codoped Tin oxide NPs synthesized via a green approach and to examine the anticancer potential of $SnNiCoO_2$ NPs in human leukemic cells. The impact of NPs administration on the cell viability, intracellular ROS, MMP level, apoptotic cell death potential, and caspases activities were analyzed and reported.

As a result, we tested the antioxidative and oxidative functions of $SnNiCoO_2$ NPs by exposing cells with diverse concentrations and measuring MDA and antioxidants (glutathione, SOD, and Catalase). Exposure of Molt-4 cells to diverse concentrations of $SnNiCoO_2$ NPs (40 and 50 µg/ml) increased intracellular MDA levels while decreasing glutathione levels, suggesting that $SnNiCoO_2$ NPs may cause oxidative injury in cells. $SnNiCoO_2$ NPs also elevated MDA levels at dose dependently. Furthermore, an elevation in the inflammatory mediators i.e., TNF-α and IL1β shows that $SnNiCoO_2$ NP exposure causes inflammation in Molt-4 cells.

From our results, the PL spectra of the $SnNiCoO_2$ NPs show peaks at wavelengths 522 nm and 527 nm. More oxygen vacancies were observed in the $SnNiCoO_2$ NPs, resulting in a higher amount of ROS. On the other hand, $Ni^{2+}/Co^{2+}/Sn^{4+}$ ions released by $SnNiCoO_2$ NPs come in contact with microbial cell membranes, and the cell membranes with a negative charge and $Ni^{2+}/Co^{2+}/Sn^{4+}$ ions with positive charge attract. As a result, the $Ni^{2+}/Co^{2+}/Sn^{4+}$ metal ions penetrate and hook onto the cell membrane and react with sulfhydryl groups within the cell membrane, which results in the cell death of the bacteria (Pandimurugan et al., 2021; Torki et al., 2022).

The cell viability analysis is one of the most essential tools for nanotoxicology investigation since it shows the cells' response to the stimulants or toxicants and transfer signal on cell survival and death rate (Kummara et al., 2016; Tabrez et al., 2022(b); Tabrez et al., 2022(c)). The leukemic cells treated with $SnNiCoO_2$ NPs revealed a considerable reduction in the viability. The outcome is in agreement with an earlier report on green un-doped and co-doped tin oxide NPs, where it was observed that the cytotoxic nature of the co-doped NPs was better than that of the un-doped NPs (Khan et al., 2018). Also, Green AgNPs synthesized from *Eucalyptus chapmaniana* leaf extract have been shown to have a notable cytotoxic impact on human leukemia in previous investigations (Sulaiman et al., 2013).

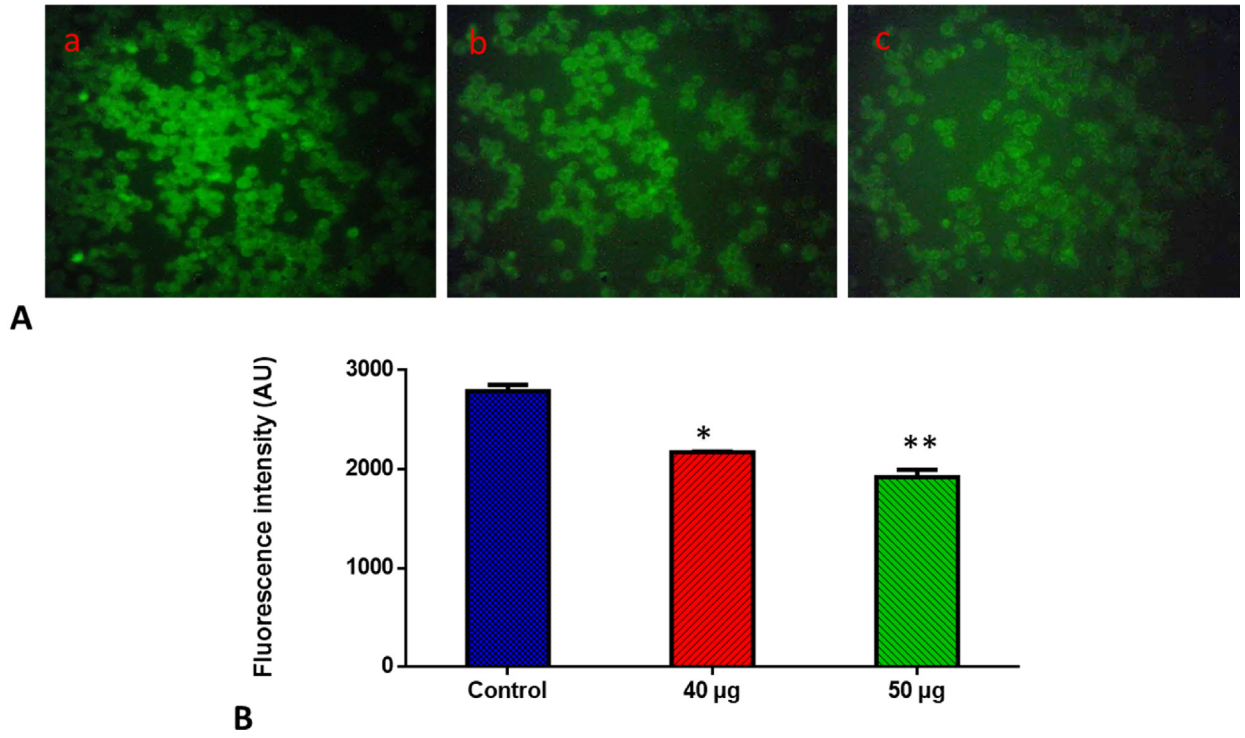


**Fig. 9** Effects of SnNiCoO2 NPs on the mitochondrial membrane potential in the blood cancer MOLT-4 cells. MOLT-4 cells with SnNiCoO2 NPs present have a decreased mitochondrial membrane permeability. Rhodamine 123 was used to stain the cells. The fluorescent images were captured by a Fluorescence microscope (Labomed, USA). Control cells showed a bright fluorescence that indicates a higher MMP level. The SnNiCoO2 NPs (40 and 50 µg/ml) treated cells showed a dull or decreased green fluorescence, which indicates the reduced MMP level in MOLT-4 cells. Panel A; Control (a) (untreated cells), SnNiCoO2 NPs-treated cells; 40 µg/ml concentration (b) and 50 µg/ml concentration (c). Panel B; Arbitrary Units (a.u.) of fluorescent Intensity from the control and treated cells incubated at 37 °C were measured by a fluorescence microplate reader. *p < 0.05 compared to the "Control" group and **p < 0.005 compared to the "Control" group.

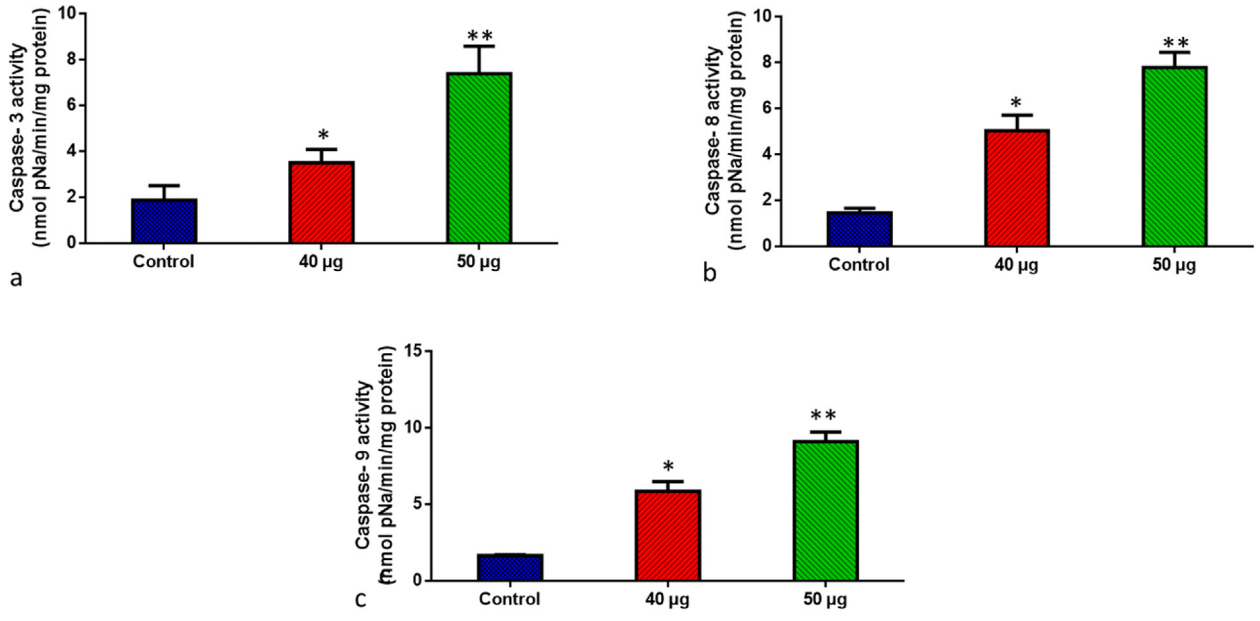


**Fig. 10** SnNiCoO2 NPs induced pro-apoptotic response Caspase −3, 8, and 9 in the MOLT-4 cell line. The colorimetric quantification of active Caspase-3 (a), Caspase-8 (b), and Caspase-9 (c) in MOLT-4 cell line after 24-h treatment of 40 and 50 µg/ml concentration of SnNiCoO2 NPs. The data were presented as activity of caspase – 3, 8, and 9 enzymes and mean ± SEM. n = 6, *p < 0.05 compared to the "Control" group and **p < 0.005 compared to the "Control" group.

The generation of intracellular ROS often leads to the initiation of oxidative stress that ultimately triggers apoptosis (Ivanova et al., 2016). The free radical formation and the subsequent build-up of oxidative stress is the fundamental process of NP toxicity. The current results notably elevated the ROS generation, which is agreement with an earlier study wherein green gold NPs demonstrated potential anticancer activity against colon cancer cells by enhancing ROS production (Malaikolundhan et al., 2020).

The AO/EB staining technique was employed to evaluate the morphological modifications concerning apoptosis to better comprehend the process of cell death induced by NPs. It was observed that the live cells exhibited green fluorescence owing to the diffusion of acridine orange into the cellular membranes whereas the apoptotic cells were represented as orange entities owing to nuclear shrinkage, which is following earlier studies conducted with green silver nanoparticles. The apoptotic bodies were formed as a result of chromatin condensation within the nucleus (Prasannaraj et al., 2016).

Mitochondria are the predominant source of intracellular ROS, therefore a lack of anti-oxidants, along with an increase in ROS levels, open up a mitochondrial transition pore, lowering MMP and triggering a caspase cascade that finally results in cell death (Nakkala et al., 2018). The level of MMP was examined to elucidate the apoptotic mechanism in the NP-treated leukemic cells. Increased ROS levels promoted mitochondrial membrane depolarization, which in turn activated the apoptotic mechanisms. An earlier investigation associated with the anticancer effect of $SnO_2$-doped ZnO NPs in breast cancer cells also revealed a similar MMP depletion trend in a dose-dependent manner (Ahamed et al., 2021).

Apoptosis, being an essential regulator of cellular homeostasis, is induced by a controlled and coordinated action of caspases (Czabotar et al., 2014; Tabrez et al., 2020(a); Tabrez et al., 2020(b)). The caspase protein family is activated by caspase-3 that stimulates apoptotic cell death by activating caspase-8 and −9 (Herr et al., 2018). $SnNiCoO_2$ NPs remarkably augmented the expressions of caspase-3, −8, and −9. Our outcomes indicate the cytotoxicity of $SnNiCoO_2$ NPs to the leukemic cells. The elevated ROS level causes mitochondrial outer membrane pores to be disrupted which decreases MMP, releasing apoptotic caspases that ultimately lead to cell death (Chen et al., 2016). Caspase-dependent apoptotic cell death facilitated by the mitochondrial route has been observed in zinc oxide NPs in squamous cancer cells (Wang et al., 2020).

## 5. Conclusion

Nanoparticles doped with green nickel and cobalt (SnNiCoO2) have been investigated for their anticancer effects on Molt-4 cells. In addition to their cytotoxic effect, the NPs also significantly increased the level of ROS and antioxidants, reduced MMP levels, and elevated caspase-3, −9, and −8 expression. As a result of the increased caspase-3, −9, and −8 expressions and the reduction of MMP, the NPs triggered apoptosis in leukemic cells. Apoptotic induction via mitochondria was found to mediate the cytotoxicity of NPs. Using SnNiCoO2 nanoparticles as a model, we have found that using a different approach can enhance their properties and anticancer capabilities. These findings indicate that nickel and cobalt-codoped tin oxide nanoparticles from Psidium guajava induce mitochondrial oxidative stress and may prove to be potential antibiotic, antifungal, and anticancer candidates.

## Declaration of Competing Interest

The authors declare that they have no known competing financial interests or personal relationships that could have appeared to influence the work reported in this paper.

## Acknowledgments

This study was supported in part by grant number (DSR-2021-01-0359) from the Deanship for Scientific Research at Jouf University.

## References

Abdelghany, T.M., Al-Rajhi, A.M., Al Abboud, M.A., Alawlaqi, M. M., Magdah, A.G., Helmy, E.A., Mabrouk, A.S., 2018. Recent advances in green synthesis of silver nanoparticles and their applications: about future directions. a review. Bionanoscience 8 (1), 5–16.

Agrahari, V., Tripathi, A.K., Mathpal, M.C., Pandey, A.C., Mishra, S.K., Shukla, R.K., Agarwal, A., 2015. Effect of Mn doping on structural, optical and magnetic properties of $SnO_2$ nanoparticles. J. Mater. Sci. Mater. Electron. 26 (12), 9571–9582.

Ahamed, M., Akhtar, M.J., Majeed Khan, M.A., Alhadlaq, H.A., 2018. Oxidative stress mediated cytotoxicity of tin (IV) oxide (SnO2) nanoparticles in human breast cancer (MCF-7) cells. Colloids Surf. B Biointerfaces 1 (172), 152–160.

Ahamed, M., Akhtar, M.J., Khan, M.A.M., Alhadlaq, H.A., 2021. SnO2-doped ZnO/reduced graphene oxide nanocomposites: synthesis, characterization, and improved anticancer activity via oxidative stress pathway. Int. J. Nanomed. 16, 89–104.

Ahmed, S., Chaudhry, S.A., Ikram, S., 2017. A review on biogenic synthesis of ZnO nanoparticles using plant extracts and microbes: a prospect towards green chemistry. J. Photochem. Photobiol. B 1 (166), 272–284.

Alserihi, R., Mohammed, M., Kaleem, M., Khan, M., Sechi, M., Sanna, V., Zughaibi, T., Abuzenadah, A., Tabrez, S., 2022. Development of (−)-epigallocatechin-3-gallate-loaded folate receptor-targeted nanoparticles for prostate cancer treatment. Nanotechnol. Rev. 11 (1), 298–311. https://doi.org/10.1515/ntrev-2022-0013.

Amutha, T., Rameshbabu, M., Florence, S.S., Senthilkumar, N., Potheher, I.V., Prabha, K., 2019. Studies on structural and optical properties of pure and transition metals (Ni, Fe, and co-doped Ni–Fe) doped tin oxide ($SnO_2$) nanoparticles for anti-microbial activity. Res. Chem. Intermed. 45 (4), 1929–1941.

Antony, J.J., Sithika, M.A., Joseph, T.A., Suriyakalaa, U., Sankarganesh, A., Siva, D., Kalaiselvi, S., Achiraman, S., 2013. In vivo antitumor activity of biosynthesized silver nanoparticles using Ficus religiosa as a nanofactory in DAL induced mice model. Colloids Surf. B Biointerfaces 1 (108), 185–190.

Bahmani, F., Esmaeili, S., Bashash, D., Dehghan-Nayeri, N., Mashati, P., Gharehbaghian, A., 2018. Centaurea albonitens extract enhances the therapeutic effects of Vincristine in leukemic cells by inducing apoptosis. Biomed. Pharmacother. 99, 598–607.

Barbalho, S.M., Farinazzi-Machado, F.M., de Alvares, G.R., Brunnati, A.C., Otoboni, A.M., Ottoboni, B.J., 2012. Psidium guajava (Guava): a plant of multipurpose medicinal applications. Med. Aromat. Plants 1 (104), 2167–10412.

Basnet, P., Chanu, T.I., Samanta, D., Chatterjee, S., 2018. A review on bio-synthesized zinc oxide nanoparticles using plant extracts as reductants and stabilizing agents. J. Photochem. Photobiol. B 1 (183), 201–221.

Bhuvana, S., Ramalingam, H.B., Thilakavathi, G., Vadivel, K., 2017. Structural, optical and magnetic properties of (Ni–Mn) co-doped tin oxide nanoparticles. Mater. Technol. 32 (5), 305–309.

Chakravarty, R., Chakraborty, S., Shukla, R., Bahadur, J., Ram, R., Mazumder, S., Sarma, H.D., Tyagi, A.K., Dash, A., 2016. Mechanochemical synthesis of mesoporous tin oxide: a new generation nanosorbent for 68 Ge/68 Ga generator technology. Dalton Trans. 45 (34), 13361–13372.

Chao, M.W., Lai, M.J., Liou, J.P., Chang, Y.L., Wang, J.C., Pan, S. L., Teng, C.M., 2015. The synergic effect of vincristine and vorinostat in leukemia in vitro and in vivo. J. Hematol. Oncol. 10 (8), 82.

Chavali, M.S., Nikolova, M.P., 2019. Metal oxide nanoparticles and their applications in nanotechnology. SN Appl. Sci. 1 (6), 1–30.

Chen, S., Hsu, C., Tsai, M., Chen, R., 2013. Inhibition of oxidative stress by low-molecular-weight polysaccharides with various functional groups in skin fibroblasts. Int. J. Mol. Sci. 14, 19399–19415.

Chen, G., Li, S.Y., Malik, H.T., Ma, Y.G., Xu, H., Sun, L.K., 2016. Organic two-photon nanoparticles modulate reactive oxygen species, intracellular calcium concentration, and mitochondrial membrane potential during apoptosis of human gastric carcinoma SGC-7901 cells. Biotechnol. Lett. 38 (8), 1269–1276.

Czabotar, P.E., Lessene, G., Strasser, A., Adams, J.M., 2014. Control of apoptosis by the BCL-2 protein family: implications for physiology and therapy. Nat. Rev. Mol. Cell Biol. 15 (1), 49–63.

Divya, J., Pramothkumar, A., Gnanamuthu, S.J., Victoria, D.B., 2020. Structural, optical, electrical, and magnetic properties of Cu and Ni-doped SnO2 nanoparticles prepared via Co-precipitation approach. Phys. B Condens. Matter. 1, (588) 412169.

Elango, G., Kumaran, S.M., Kumar, S.S., Muthuraja, S., Roopan, S. M., 2015. Green synthesis of $SnO_2$ nanoparticles and its photocatalytic activity of phenolsulfonphthalein dye. Spectrochim. Acta A Mol. Biomol. Spectrosc. 15 (145), 176–180.

Ghramh, H.A., Khan, K.A., Ibrahim, E.H., 2019. Biological activities of Euphorbia peplus leaves ethanolic extract and the extract fabricated gold nanoparticles (AuNPs). Molecules 24 (7), 1431.

Gowd V, Ahmad A, Tarique M, Suhail M, Zughaibi TA, Tabrez S, Khan R. Advancement of cancer immunotherapy using nanoparticles-based nanomedicine. Semin Cancer Biol. 2022 Apr 1;86(Pt 2):624-644. doi: 10.1016/j.semcancer.2022.03.026. Epub ahead of print. PMID: 35378274.

Herr, A.B., 2018. Evolution of an allosteric "off switch" in apoptotic caspases. J. Biol. Chem. 293 (15), 5462–5463.

Ivanova, D., Zhelev, Z., Aoki, I., Bakalova, R., Higashi, T., 2016. Overproduction of reactive oxygen species-obligatory or not for induction of apoptosis by anticancer drugs. Chinese J. Cancer Res. 28 (4), 383.

Iyappan, P., Bala, M.D., Sureshkumar, M., Veeraraghavan, V.P., Palanisamy, A., 2021. D-carvone induced ROS mediated apoptotic cell death in human leukemic cell lines (Molt-4). Bio information 17 (1), 171–180.

Khan, S.A., Kanwal, S., Rizwan, K., Shahid, S., 2018. Enhanced antimicrobial, antioxidant, in vivo antitumor and in vitro anticancer effects against breast cancer cell line by green synthesized un-doped SnO2 and Co-doped SnO2 nanoparticles from Clerodendrum inerme. Microb. Pathog. 1 (125), 366–384.

Khan, A.K., Renouard, S., Drouet, S., Blondeau, J.P., Anjum, I., Hano, C., Abbasi, B.H., Anjum, S., 2021. Effect of UV irradiation (A and C) on casuarina equisetifolia-mediated biosynthesis and characterization of antimicrobial and anticancer activity of biocompatible zinc oxide nanoparticles. Pharmaceutics 13 (11), 1977.

Khan, K., Tareen, A.K., Iqbal, M., Mahmood, A., Shi, Z., Yin, J., Qing, D., Ma, C., Zhang, H., 2021. Recent development in graphdiyne and its derivative materials for novel biomedical applications. J. Mater. Chem. B.

Khojasteh, F., Mersagh, M.R., Hashemipour, H., 2022. The influences of Ni, Ag-doped $TiO_2$ and $SnO_2$, Ag-doped $SnO_2/TiO_2$ nanocomposites on recombination reduction in dye synthesized solar cells. J. Alloy. Compd. 890, 161709.

Kummara, S., Patil, M.B., Uriah, T., 2016. Synthesis, characterization, biocompatible and anticancer activity of green and chemically synthesized silver nanoparticles–a comparative study. Biomed. Pharmacother. 1 (84), 10–21.

Malaikolundhan, H., Mookkan, G., Krishnamoorthi, G., Matheswaran, N., Alsawalha, M., Veeraraghavan, V.P., Krishna Mohan, S., Di, A., 2020. Anticarcinogenic effect of gold nanoparticles synthesized from Albizia lebbeck on HCT-116 colon cancer cell lines. Artif. Cells Nanomed. Biotechnol. 48 (1), 1206–1213.

Mittal, J., Batra, A., Singh, A., Sharma, M.M., 2014. Phytofabrication of nanoparticles through plant as nanofactories. Adv. Nat. Sci. Nanosci. Nanotechnol. 5, (4) 043002.

Mosmann, T., 1983. Rapid colorimetric assay for cellular growth and survival: application to proliferation and cytotoxicity assays. J. Immunol. Methods 65 (1–2), 55–63.

Mostafa, A.M., Mwafy, E.A., 2020. Effect of dual-beam laser radiation for synthetic SnO2/Au nanoalloy for antibacterial activity. J. Mol. Struct. 15, (1222) 128913.

Naje, A.N., Norry, A.S., Suhail, A.M., 2013. Preparation and characterization of $SnO_2$ nanoparticles. Int. J. Innov. Res. Sci. Eng. Technol. 2, 7068–7072.

Nakkala, J.R., Mata, R., Raja, K., Chandra, V.K., Sadras, S.R., 2018. Green synthesized silver nanoparticles: catalytic dye degradation, in vitro anticancer activity and in vivo toxicity in rats. Mater. Sci. Eng. C 1 (91), 372–381.

Nguyen, D.H., Vo, T.N., Nguyen, N.T., Ching, Y.C., Hoang Thi, T. T., 2020. Comparison of biogenic silver nanoparticles formed by Momordica charantia and Psidium guajava leaf extract and antifungal evaluation. Plos one 15 (9), e0239360.

Nikbakht, M., Jha, A.K., Malekzadeh, K., Askari, M., Mohammadi, S., Marwaha, R.K., Kaul, D., Kaur, J., 2017. Aberrant promoter hypermethylation of selected apoptotic genes in childhood acute lymphoblastic leukemia among North Indian population. Exp. Oncol. 39 (1), 57–64.

Pal, K., Si, A., El-Sayyad, G.S., Elkodous, M.A., Kumar, R., El-Batal, A.I., Kralj, S., Thomas, S., 2021. Cutting edge development on graphene derivatives modified by liquid crystal and $CdS/TiO_2$ hybrid matrix: optoelectronics and biotechnological aspects. Crit. Rev. Solid State Mater. Sci. 46 (5), 385–449.

Pandimurugan, A.R., Sankaranarayanan, K., 2021. Antibacterial and photocatalytic activity of ZnO, $SnO_2$ and $Zn_2SnO_4$ nanoparticles prepared by microwave assisted method. Mater. Technol., 1–11

Pascariu, P., Airinei, A., Grigoras, M., Fifere, N., Sacarescu, L., Lupu, N., Stoleriu, L., 2016. Structural, optical and magnetic properties of Ni-doped $SnO_2$ nanoparticles. J. Alloys Compd. 25 (668), 65–72.

Prasannaraj, G., Sahi, S.V., Ravikumar, S., Venkatachalam, P., 2016. Enhanced cytotoxicity of biomolecules loaded metallic silver nanoparticles against human liver (HepG2) and prostate (PC3) cancer cell lines. J. Nanosci. Nanotechnol. 16 (5), 4948–4959.

Prashanth, G.K., Prashanth, P.A., Nagabhushana, B.M., Ananda, S., Krishnaiah, G.M., Nagendra, H.G., Sathyananda, H.M., Rajendra Singh, C., Yogisha, S., Anand, S., Tejabhiram, Y., 2018. Comparison of anticancer activity of biocompatible ZnO nanoparticles prepared by solution combustion synthesis using aqueous leaf extracts of Abutilon indicum, Melia azedarach and Indigofera tinctoria as biofuels. Artif. Cells Nanomed. Biotechnol. 46 (5), 968–979.

Rani, N., Khurana, K., Jaggi, N., 2021. Spectroscopic analysis of $SnO_2$ nanoparticles attached functionalized multiwalled carbon nanotubes. Surf. Interfaces 27, 101492.

Sephra, P.J., Baraneedharan, P., Siva, C., Sivakumar, M., Nehru, K., 2016. Microwave assisted synthesis of $Sn_{(1-x)}CoxO_2$ nanoparticles: effect of impurity phase formation on structural, optical and electrochemical properties. J. Mater. Sci.: Mater. Electron. 27 (11), 11401–11409.

SPSS Inc. Released 2008. SPSS Statistics for Windows, Version 17.0. Chicago: SPSS Inc.

Srinivas, K., Vithal, M., Sreedhar, B., Raja, M.M., Reddy, P.V., 2009. Structural, optical, and magnetic properties of nanocrystalline Co doped $SnO_2$-based diluted magnetic semiconductors. J. Phys. Chem. C 113 (9), 3543–3552.

Sulaiman, G.M., Mohammed, W.H., Marzoog, T.R., Al-Amiery, A. A., Kadhum, A.A., Mohamad, A.B., 2013. Green synthesis, antimicrobial and cytotoxic effects of silver nanoparticles using Eucalyptus chapmaniana leaves extract. Asian Pac. J. Trop. Biomed. 3 (1), 58–63.

Suwan, T., Khongkhunthian, S., Okonogi, S., 2019. Antifungal activity of polymeric micelles of silver nanoparticles prepared from Psidium guajava aqueous extract. Drug Discov. Ther. 13 (2), 62–69.

Tabrez S, Jabir NR, Khan MI, Khan MS, Shakil S, Siddiqui AN, Zaidi SK, Ahmed BA, Kamal MA. Association of autoimmunity and cancer: An emphasis on proteolytic enzymes. Semin Cancer Biol. 2020(b) Aug;64:19-28. doi: 10.1016/j.semcancer.2019.05.006. Epub 2019 May 14. PMID: 31100322.

Tabrez S, Jabir NR, Adhami VM, Khan MI, Moulay M, Kamal MA, Mukhtar H. Nanoencapsulated dietary polyphenols for cancer prevention and treatment: successes and challenges. Nanomedicine (Lond). 2020 (a) May;15(11):1147-1162. doi: 10.2217/nnm-2019-0398. Epub 2020 Apr 15. PMID: 32292109.

Tabrez S, Khan A, Hoque M, Suhail M, Khan M, Zughaibi T. Biosynthesis of ZnO NPs from pumpkin seeds' extract and elucidation of its anticancer potential against breast cancer. Nanotechnology Reviews. 2022 (a);11(1): 2714-2725. https://doi.org/10.1515/ntrev-2022-0154

Tabrez S, Khan A, Mirza A, Suhail M, Jabir N, Zughaibi T, Alam M. Biosynthesis of copper oxide nanoparticles and its therapeutic efficacy against colon cancer. Nanotechnology Reviews. 2022 (b);11(1): 1322-1331. https://doi.org/10.1515/ntrev-2022-0081

Tabrez S, Khan AU, Hoque M, Suhail M, Khan MI, Zughaibi TA. Investigating the anticancer efficacy of biogenic synthesized MgONPs: An in vitro analysis. Front Chem. 2022(c) Sep 15;10:970193. doi: 10.3389/fchem.2022.970193. PMID: 36186592; PMCID: PMC9520594.

Toloman, D., Popa, A., Stefan, M., Silipas, T.D., Suciu, R.C., Barbu-Tudoran, L., Pana, O., 2020. Enhanced photocatalytic activity of Co doped $SnO_2$ nanoparticles by controlling the oxygen vacancy states. Opt. Mater. 110, 110472.

Ullah, F., Shah, K.U., Shah, S.U., Nawaz, A., Nawaz, T., Khan, K. A., Alserihi, R.F., Tayeb, H.H., Tabrez, S., Alfatama, M., 2022. Synthesis, characterization and in vitro evaluation of chitosan nanoparticles physically admixed with lactose microspheres for pulmonary delivery of montelukast. Polymers 14 (17), 3564. https://doi.org/10.3390/polym14173564.

Wang, L.S.W., Lee, C.H., Lin, M.S., Chi, C.W., Chen, Y.J., Wang, G. S., Liao, K.W., Chiu, L.P., Wu, S.H., Huang, D.M., Chen, L., Shen, Y.S., 2020. ZnO nanoparticles induced caspase-dependent apoptosis in gingival squamous cell carcinoma through mitochondrial dysfunction and p70S6K signaling pathway. Int. J. Mol. Sci. 21 (5), E1612.

Wang, L., Wu, Y., Xie, J., Wu, S., Wu, Z., 2018. Characterization, antioxidant and antimicrobial activities of green synthesized silver nanoparticles from *Psidium guajava* L. leaf aqueous extracts. Mater. Sci. Eng. C 1 (86), 1–8.